Scattering of ^{3}He atoms from ^{4}He surfaces

E. Krotscheck and R. Zillich
Institut für Theoretische Physik, Johannes Kepler Universität, A 4040 Linz, Austria
(Received 20 February 1998)

We develop a first-principles, microscopic theory of impurity atom scattering from inhomogeneous quantum liquids such as adsorbed films, slabs, or clusters of ^{4}He. The theory is built upon a quantitative, microscopic description of the ground state of both the host liquid as well as the impurity atom. Dynamic effects are treated by allowing all ground-state correlation functions to be time dependent. Our description includes both the elastic and inelastic coupling of impurity motion to the excitations of the host liquid. As a specific example, we study the scattering of ^{3}He atoms from adsorbed ^{4}He films. We examine the dependence of ''quantum reflection'' on the substrate, and the consequences of impurity bound states, resonances, and background excitations for scattering properties. A thorough analysis of the theoretical approach and the physical circumstances point towards the essential role played by inelastic processes which determine almost exclusively the reflection probabilities. The coupling to impurity resonances within the film leads to a visible dependence of the reflection coefficient on the direction of the impinging particle. [S0163-1829(98)01033-9]

I. INTRODUCTION

Dynamic scattering processes of helium atoms from low-temperature liquid ^{4}He films and the bulk fluid in the vicinity of a free surface continue to be a subject of considerable interest. Experimental information is available mostly for ^{4}He scattering processes, connected with quantum reflection and quantum evaporation,[1–4] as well as the surface reflectivity.[5–8,1] Due to experimental difficulties, there are only few data for ^{3}He scattering,[9] but there is also interest (experimental,[10–13] and theoretical[14–16]) in the dynamics of hydrogen atoms on ^{4}He surfaces for which our theory also applies.

This paper follows up on a line of work studying the properties and the dynamic features of quantum liquid films from a manifestly microscopic point of view. Most relevant for the present work are papers designing the theory for the background host liquid,[17] its excitations,[18,19] and the dynamics of atomic impurities.[20] In that work, we have used the method of correlated variational wave functions which has in many situations proven to be a computationally efficient, precise, and robust method for the purpose of studying strongly interacting quantum liquids. Even the simplest approximation of the theory has in the past given quite satisfactory results on the nature of the impurity states,[21] their effective mass,[22] and the impurity-impurity interaction[23] in inhomogeneous geometries. The reason for the *qualitative* success of the theory is that it contains a consistent treatment of both the short- and the long-range structure of the system. This implies that both the low- and the high-lying excitations are treated accurately.

The present paper complements a similar study of the scattering of ^{4}He atoms from ^{4}He slabs;[24] the problem at hand is somewhat simpler since there is no need to fully symmetrize the wave function of the background system *and* the impinging particle. Another major physical difference to the scattering of ^{4}He particles is that in the latter case one might observe[25–27] the coupling to the Bose-Einstein condensate, whereas in the present case one can couple both to phononlike and to single-particle excitations. Nevertheless we will see that many similarities exist between the two problems: The scattering process is dominated by inelastic channels, mostly the coupling to ripplonic excitations.

Generally, the impinging particle can, in the presence of other particles like the film of ^{4}He under consideration here, scatter into three types of channels:

(1) Elastic reflection: The incoming particle, characterized by the wave vector $(\mathbf{k}_\parallel, k_\perp)$, is elastically reflected with a probability $|R|^2$. It creates virtual excitations of the background, but transfers no energy.

(2) Inelastic scattering: with a probability $r_{\rm inel}$ the particle loses some energy to an excitation of the film, and retains enough energy to leave the attractive potential of the film and the substrate. The film excitation can be either a collective wave (ripplon, phonon), or a single ^{4}He that is elevated above the chemical potential μ_4 and leaves the film. The creation of several excitations is, in principle, also included in our theoretical description, but it is ignored in the linearized treatment of the equations of motion.

(3) Adsorption: as in the previous case, the film is excited, but the particle is adsorbed to the film. The corresponding *sticking coefficient* s is the probability for this process.

These three types of processes are depicted in Fig. 1. Because of the hermiticity of the *many-body* Hamiltonian for N ^{4}He atoms and the ^{3}He impurity, we have

$$|R|^2 + r_{\rm inel} + s = 1. \tag{1.1}$$

This work focuses on the calculation of elastic scattering because the impinging particle couples, in particular at low energies, predominantly to the low-lying, bound excitations of the background film and the impurity atom. We shall argue below that, basically for phase-space reasons, inelastic processes are expected to be less important than either elastic, or total absorption processes.

Since most of the theoretical tools of the present study have been derived in Ref. 20, we outline in Sec. II only briefly the theoretical methods and the basic equations to be

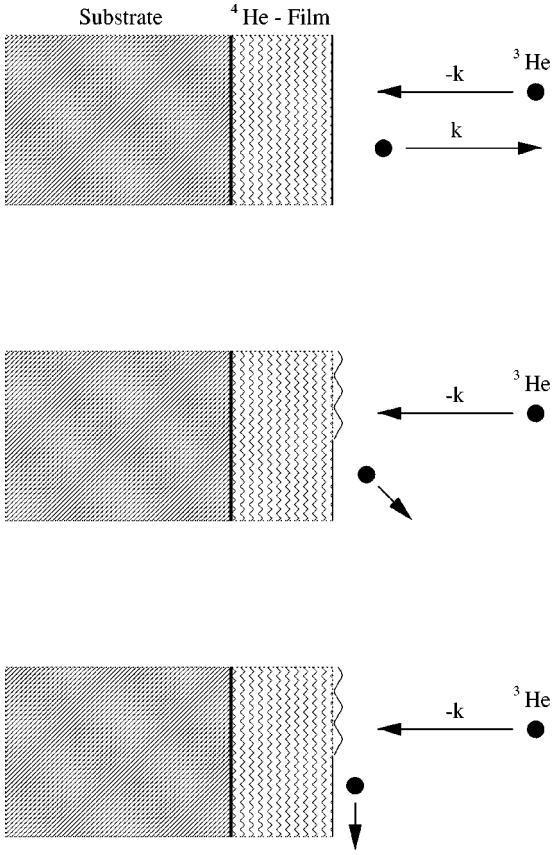

FIG. 1. The three classes of scattering channels are illustrated. The incoming particle can be (a) scattered elastically (top figure), (b) inelastically (middle figure), or (c) adsorbed to the film (bottom figure).

solved. The scattering problem will be be formulated in terms of a nonlocal, energy-dependent ''optical potential'' which depends explicitly on the coupling of the impinging particle to background and impurity excitations.

The results of our calculations are discussed in Sec. IV. To cover a variety of physical situations, we will present results for several of the systems that were studied extensively in our previous calculations: These will range from strongly bound films on a model graphite substrate that is covered with two layers of solid helium, to a very weakly bound model, described by a rather thick, metastable film on a cesium substrate. We first discuss the possible excitations of the background systems, and then present results for the surface reflectivity as a function of impact energy and angle for some of those systems. At very low energies, we will encounter the effect of ''quantum reflection;''[28–30,16,31,14,15] with increasing impact energies we also can analyze the influence of surface excitations (ripplons) and the Andreev state, phonon/roton creation, and under certain circumstance the coupling to an ''Andreev resonance'' of the impurity particle close to the substrate.

II. MICROSCOPIC THEORY

The theoretical description of ^{4}He films and impurity properties starts with a description of the ground state of the background system. Next, a single impurity is added, and finally this impurity is allowed to move. The technical derivation and in particular the important verification of our theoretical tools have been presented in a series of previous papers,[32,17,20] we will therefore discuss the theoretical background only briefly.

A. The background liquid

In the first step, one calculates the properties of the background helium film. The only phenomenological input to the theory is the microscopic Hamiltonian

$$H_N=\sum_{1\leqslant i\leqslant N}\left[-\frac{\hbar^2}{2m_B}\nabla_i^2+U_{\rm sub}(\mathbf{r}_i)\right]+\sum_{1\leqslant i<j\leqslant N}V(|\mathbf{r}_i-\mathbf{r}_j|), \tag{2.1}$$

where $V(|\mathbf{r}_i-\mathbf{r}_j|)$ is the ^{4}He-^{4}He interaction, and $U_{\rm sub}(\mathbf{r})$ is the external ''substrate'' potential. The many-body wave function is modeled by the *Jastrow-Feenberg ansatz*

$$\Psi_N(\mathbf{r}_1,\ldots,\mathbf{r}_N)=\exp\frac{1}{2}\left[\sum_{1\leqslant i\leqslant N}u_1(\mathbf{r}_i)+\sum_{1\leqslant i<j\leqslant N}u_2(\mathbf{r}_i,\mathbf{r}_j)+\sum_{1\leqslant i<j<k\leqslant N}u_3(\mathbf{r}_i,\mathbf{r}_j,\mathbf{r}_k)\right]. \tag{2.2}$$

An essential part of the method is the *optimization* of the many-body correlations by solving the Euler equations

$$\frac{\delta E_N}{\delta u_n}(\mathbf{r}_1,\ldots,\mathbf{r}_n)=0 \quad (n=1,2,3), \tag{2.3}$$

where E_N is the energy expectation value of the N-particle Hamiltonian (2.1) with respect to the wave function (2.2),

$$E_N=\frac{\int d^3r_1\ldots d^3r_N\Psi_N(\mathbf{r}_1,\ldots,\mathbf{r}_N)H_N\Psi_N(\mathbf{r}_1,\ldots,\mathbf{r}_N)}{\int d^3r_1\ldots d^3r_N\Psi_N^2(\mathbf{r}_1,\ldots,\mathbf{r}_N)}. \tag{2.4}$$

The energy is evaluated using the hypernetted chain (HNC) hierarchy of integral equations;[33] ''elementary diagrams'' and triplet correlations have been treated as described in Ref. 17.

The HNC equations also provide relationships between the *correlation functions* $u_n(\mathbf{r}_1,\ldots,\mathbf{r}_n)$ and the corresponding n-body densities. One of the quantities of primary interest is the pair-distribution function $g(\mathbf{r}_1,\mathbf{r}_2)$ and the associated (real-space) static structure function

$$S(\mathbf{r}_1,\mathbf{r}_2)=\delta(\mathbf{r}_1-\mathbf{r}_2)+\sqrt{\rho_1(\mathbf{r}_1)\rho_1(\mathbf{r}_2)}[g(\mathbf{r}_1,\mathbf{r}_2)-1]. \tag{2.5}$$

The static structure function and the effective one-body Hamiltonian

$$H_1(\mathbf{r})=-\frac{\hbar^2}{2m_B}\frac{1}{\sqrt{\rho_1(\mathbf{r})}}\nabla\rho_1(\mathbf{r})\nabla\frac{1}{\sqrt{\rho_1(\mathbf{r})}} \tag{2.6}$$

define the *Feynman excitation spectrum* through the generalized eigenvalue problem

$$H_1(\mathbf{r}_1)\psi^{(l)}(\mathbf{r}_1)=\hbar\omega_l\int d^3r_2S(\mathbf{r}_1,\mathbf{r}_2)\psi^{(l)}(\mathbf{r}_2), \tag{2.7}$$

which is readily identified with the inhomogeneous generalization[34] of the well-known Feynman dispersion relation[49] $\hbar\omega(k)=\hbar^2k^2/2m_BS(k)$. The states $\psi^{(l)}(\mathbf{r})$, their associated energies $\hbar\omega_l$, and the adjoint states

$$\phi^{(l)}(\mathbf{r})=\frac{1}{\hbar\omega_l}H_1(\mathbf{r})\psi^{(l)}(\mathbf{r}) \tag{2.8}$$

are useful quantities for the impurity problem and for the representation of the dynamic structure function of the background film.

B. The static impurity atom

The Hamiltonian of the $N+1$ particle system consisting of N ^{4}He atoms and one impurity is

$$H^I_{N+1}=-\frac{\hbar^2}{2m_I}\nabla_0^2+U^I_{\rm sub}(\mathbf{r}_0)+\sum_{i=1}^{N}V^I(|\mathbf{r}_0-\mathbf{r}_i|)+H_N. \tag{2.9}$$

We adopt the convention that coordinate $\mathbf{r}_0$ refers to the impurity particle and coordinates $\mathbf{r}_i$, with $i=1\ldots N$ to the background particles. Note that the substrate potentials $U_{\rm sub}(\mathbf{r}_i)$ and $U^I_{\rm sub}(\mathbf{r}_0)$, as well as the interactions $V^I(|\mathbf{r}_0-\mathbf{r}_j|)$ and $V(|\mathbf{r}_i-\mathbf{r}_j|)$, can be different functions for different particle species.

The generalization of the wave function (2.2) for an inhomogeneous N-particle Bose system with a single impurity atom is

$$\Psi^I_{N+1}(\mathbf{r}_0,\mathbf{r}_1,\ldots,\mathbf{r}_N)=\exp\frac{1}{2}\Big[u^I_1(\mathbf{r}_0)+\sum_{1\le i\le N}u^I_2(\mathbf{r}_0,\mathbf{r}_i)+\sum_{1\le i<j\le N}u^I_3(\mathbf{r}_0,\mathbf{r}_i,\mathbf{r}_j)\Big]\times\Psi_N(\mathbf{r}_1,\ldots,\mathbf{r}_N). \tag{2.10}$$

The energy necessary for (or gained by) adding one impurity atom into a system of N background atoms is the impurity chemical potential

$$\mu^I\equiv E^I_{N+1}-E_N. \tag{2.11}$$

Here, E^I_{N+1} is to be understood as the energy expectation value of the Hamiltonian (2.9) with respect to the wave function (2.10). The further steps parallel those of the derivation of the background structure.

The impurity density is calculated by minimizing the chemical potential (2.11) with respect to $\sqrt{\rho^I_1(\mathbf{r}_0)}$. This leads to an effective Hartree equation

$$-\frac{\hbar^2}{2m_I}\nabla_0^2\eta^{(r)}(\mathbf{r}_0)+[U^{\rm I}_{\rm sub}(\mathbf{r}_0)+V_H(\mathbf{r}_0)]\eta^{(r)}(\mathbf{r}_0)=t_r\eta^{(r)}(\mathbf{r}_0), \tag{2.12}$$

where $V_H(\mathbf{r}_0)$ is an effective, self-consistent one-body potential for the single impurity. The lowest eigenvalue of Eq. (2.12) is the impurity chemical potential $\mu^I=t_0$, and the corresponding eigenfunction the density of the impurity ground state, $\sqrt{\rho^I_1(\mathbf{r})}=\eta^{(0)}(\mathbf{r})$.

In the systems studied below, translational invariance in the $x-y$ plane is assumed, and the states are characterized by two quantum numbers, m and $\mathbf{k}_m$, associated with the motion perpendicular (m) and parallel to the symmetry plane ($\mathbf{k}_m$). When unambiguous, as in the states $\eta^{(r)}(\mathbf{r}_0)$ and $\phi^{(m)}(\mathbf{r}_1)$, we shall use the single label (e.g., m) to collectively represent both quantum numbers. In particular, the states $\eta^{(r)}(\mathbf{r}_0)$ depend only trivially on the parallel coordinate,

$$\eta^{(r)}(\mathbf{r}_0)=\eta^{(r)}(z_0)e^{i\mathbf{k}_r\cdot\mathbf{r}_\parallel}. \tag{2.13}$$

The unit volume is chosen as the size of the normalization volume. The corresponding energies are

$$t_r=\epsilon_r+\frac{\hbar^2k_\parallel^2}{2m_I}, \tag{2.14}$$

where ϵ_r are the eigenvalues of Eq. (2.12) for $k_\parallel=0$.

C. Impurity dynamics

It is tempting to identify the higher-lying eigenstates of the ''Hartree equation'' (2.12) with the excited states of the impurity. This is legitimate only in a *static approximation* for the impurity features. However, such a simplification misses two important features:

(i) If the momentum is a good quantum number, low-lying excited states can be discussed in terms of an *effective mass.* In our geometry, a ''hydrodynamic effective mass'' is associated with the motion of an impurity particle *parallel* to the surface; it is caused by the coupling of the impurity motion to the excitations of the background liquid. The local Hartree equation (2.12) misses this effect.

(ii) The effective Hartree potential $V_H(z)$ is real, i.e., all ''excitations'' defined by the local equation (2.12) have an infinite lifetime. A more realistic theory should describe resonances and allow for their decay by the coupling to the low-lying background excitations of the host film.

Hence, a static equation of the type (2.12) is appropriate for the impurity ground state only. The natural generalization of the variational approach to a dynamic situation is to allow for time-dependent correlation functions $u_n(\mathbf{r}_0,\ldots,\mathbf{r}_n;t)$. We write the time-dependent variational wave function in the form

$$\phi(t)=\frac{1}{\sqrt{\langle\psi^I|\psi^I\rangle}}e^{-iE^I_{N+1}t/\hbar}\psi^I(\mathbf{r}_0,\mathbf{r}_1,\ldots\mathbf{r}_N;t). \tag{2.15}$$

Consistent with the general strategy of variational methods, we include the time dependence in the one-particle *and* two-particle impurity-background correlations, i.e., we write

$$\psi^I(\mathbf{r}_0,\mathbf{r}_1,\ldots\mathbf{r}_N;t)=\exp\frac{1}{2}\Big[\delta u_1(\mathbf{r}_0;t)+\sum_{1\le i\le N}\delta u_2(\mathbf{r}_0,\mathbf{r}_i;t)\Big]\times\Psi^I_{N+1}(\mathbf{r}_0,\mathbf{r}_1,\ldots,\mathbf{r}_N). \tag{2.16}$$

The time-independent part remains the same as defined in Eq. (2.10). The time-dependent correlations are determined by searching for a stationary state of the action integral

$$\mathcal{S}=\int_{t_0}^{t}\mathcal{L}(t)dt,$$
$$\mathcal{L}(t)=\left\langle \phi(t)\left| H^I_{N+1}-i\hbar\frac{\partial}{\partial t}\right|\phi(t)\right\rangle, \tag{2.17}$$

where H^I_{N+1} is the Hamiltonian (2.9) of the impurity-background system.

The derivation of a set of useful equations of motion for the impurity have been given in Ref. 20. The final result is readily (and expectedly) identified with a Green's function expression, where the three-body vertex function describes an impurity atom scattering off a phonon, and is given in terms of quantities calculated in the ground-state theory. The motion of the impurity particle is determined by an effective Schrödinger equation of the form

$$\left[-\frac{\hbar^2}{2m_I}\nabla^2+U^I_{\rm sub}+V_H(\mathbf{r})\right]\psi_I(\mathbf{r},\omega)$$
$$+\int d^3r'\Sigma(\mathbf{r},\mathbf{r}',\omega)\psi_I(\mathbf{r}',\omega)=\hbar\omega\psi_I(\mathbf{r},\omega), \tag{2.18}$$

where $V_H(\mathbf{r})$ is the effective one-body potential of Eq. (2.12), and $\Sigma(\mathbf{r},\mathbf{r}',\omega)$ is the impurity self-energy. Within the chosen level of the theory, $\Sigma(\mathbf{r},\mathbf{r}',\omega)$ describes three-body processes,

$$\Sigma(\mathbf{r},\mathbf{r}',\omega)=\sum_{rm}\frac{W_{mr}(\mathbf{r})W_{mr}(\mathbf{r}')}{\hbar\omega-\hbar\omega_m-t_r}, \tag{2.19}$$

where $W_{mr}(\mathbf{r})$ is the three-body vertex function that describes the coupling between an incoming ^{3}He particle to an outgoing ^{3}He in the state r as well as an outgoing phonon in state m. The detailed form of these matrix elements follows from the microscopic theory that has been described in length in Ref. 20, it is not illuminating for the further considerations.

The structure of Eqs. (2.18) and (2.19) is of the expected form of an energy-dependent Hartree equation with a self-energy correction involving the energy loss or gain of the impurity particle by coupling to the excitations of the background system. It is the simplest form that contains the desired physical effects.

The energy denominator in Eq. (2.19) contains the Feynman excitation energies defined in Eq. (2.7) and the Hartree impurity energies of Eq. (2.12). These energies are too high, and we expect therefore that three-body effects are somewhat underestimated. A lowering of the spectra in the energy denominator by an impurity effective mass or by a more quantitative phonon/roton spectrum should have the effect of enhancing the importance of multiparticle scattering processes. Hence, it is expected that the binding energy of the surface resonance is still somewhat too high compared with experiments. On the other hand, it is not expected that a more quantitative spectrum in the self-energy should change the effective mass of the Andreev state considerably because the hydrodynamic backflow causing this effective mass is mostly caused by the coupling to ripplons, which are well described within the Feynman approximation.

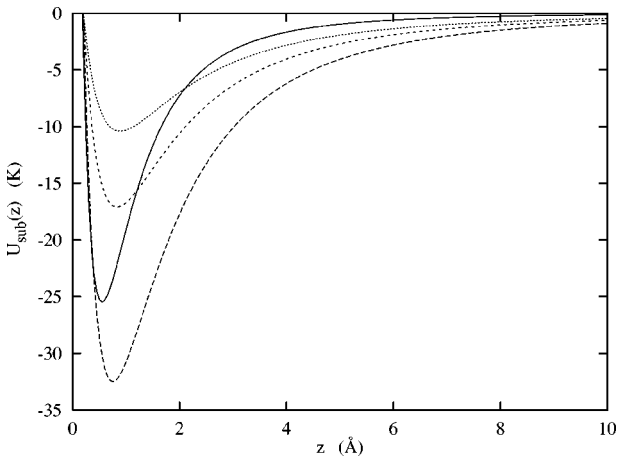

FIG. 2. The figure shows the three substrate potentials for the films under consideration here: Graphite *plus* two solid helium layers (solid line), Mg (long dashed line), Na (short dashed line) and Cs (dotted line).

III. THE PHYSICAL MODELS

We consider liquid ^{4}He adsorbed to a plane attractive substrate which is translationally invariant in the $x-y$ plane, i.e., $U_{\rm sub}(\mathbf{r})=U_{\rm sub}(z)$. The systems under consideration are characterized by the substrate potential $U_{\rm sub}(z)$ and the surface coverage

$$n=\int_0^\infty dz\rho_1(z), \tag{3.1}$$

where $\rho_1(\mathbf{r})=\rho_1(z)$ is the density profile of the ^{4}He host system. This density profile is, along with the energetics, structure functions, and excitations of the film, obtained through the optimization of the ground-state (2.2) as outlined above; the procedure has been described in detail in Ref. 17.

A. Ground state

We have in this work studied the scattering properties of ^{3}He atoms for a number of selected substrate potentials and surface coverages; we have selected four cases for the purpose of a detailed discussion. The substrate potentials and the corresponding density profiles are shown in Figs. 2 and 3. The surface coverages are $n=0.3$ Å^{-2} for each substrate potential; additionally we have considered the case $n=0.4$ Å^{-2} for a Cs substrates as well as Mg for a case that is somewhat more attractive than the screened graphite, but has a long range.

Alkali metal substrate potentials are simple 3-9 potentials characterized by their *range* C_3 and their *well depth* D. They have the form

$$U_{\rm sub}(z)=\left[\frac{4C_3^3}{27D^2}\right]\frac{1}{z^9}-\frac{C_3}{z^3}. \tag{3.2}$$

The range parameters C_3 of these potentials have been calculated by Zaremba and Kohn,[35] the short-range z^{-9} term is

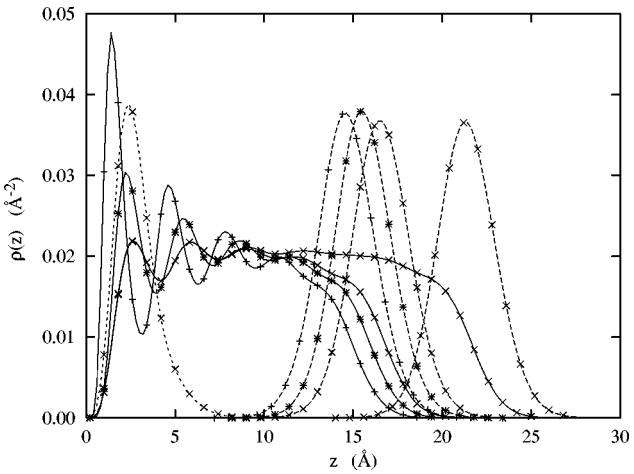

FIG. 3. The figure shows the four density profiles of the background liquid (solid lines) and the impurity location (long dashed lines) for which most of the present calculations were done. Graphite substrate results are marked with + -symbols, Na results with stars, and Cs results with crosses. Also shown is the interfacial Andreev state on a Cs substrate (short-dashed line marked with crosses). Coverages are $n=0.30$ Å^{-2} for Cs, Na, and graphite, and $n=0.40$ Å^{-2} for Cs. Profiles on Mg have been left out for clarity.

phenomenological and fitted to reproduce the binding energies of a single atom on these substrates. Slightly more complicated is our model of a graphite substrate covered with two solid layers of ^{4}He. Most important for low-energy scattering properties is the coefficient C_3 of the long-range attraction, the values of C_3 for our substrates of graphite, Cs, Na, and Mg are 180, 670, 1070, and 1750 K Å^3, respectively.[35,36] The graphite potential is relatively short-range but deep and produces a very visible layering structure of the background film; thus one obtains a rather ''stiff'' system.[17]

Figure 2 provides a comparison of these four different potentials. It is seen that the alkali-metal potentials are longer ranged, the magnesium substrate has the deepest potential well. At the opposite end of the potential strength is the Cs substrates. This substrate has received much attention in recent years because of the experimental finding that it is nonwetting.[37–39] Note that the Cs-adsorbed films are metastable; they were examined with two purposes in mind. One is to generate a situation that is reasonably close to the infinite half-space limit. Therefore, we have studied this case also for the larger surface coverage $n=0.4$ Å^{-2}. The second reason is that the nature of the low-lying excitations,[40] as well as that of the impurity states,[41] is somewhat different than those for the graphite model as will be seen below. The third case, a Na substrate, is an intermediate case which is of some interest for the nature of the ^{3}He bound states, whereas the Mg substrate is both deeper and longer ranged than the screened graphite.

B. Background excitations

Our earlier work[18,19,42] has discussed extensively the excitations of quantum liquid films adsorbed to various substrates. These studies have been concerned with the interpretation of neutron scattering experiments,[43–45] they have therefore focused on excitations propagating *parallel* to the film. Typically, four types of modes were found:

(1) *Surface excitations*: At long wavelengths and on strong substrates, these are substrate potential-driven modes with a linear dispersion relation

$$\omega_3(k)=c_3k, \tag{3.3}$$

where c_3 is the speed of *third sound*. At shorter wavelengths and in the case of an infinite half space, the surface mode is driven by the surface tension and has a dispersion relation

$$\omega_r^2(k)=\frac{\sigma}{m\rho_\infty}k^3, \tag{3.4}$$

where σ is the surface tension, and ρ_∞ is the density of the bulk liquid. In practice, the dispersion relation is linear only in a rather small momentum regime, and the ripplon dispersion relation (3.4) is a quite good approximation[42] for the surface-mode dispersion relation up to wavelengths of about 0.5 Å^{-1}. The theoretically predicted surface energy obtained from Eq. (3.4) by a $k^{3/2}$ fit to the dispersion relation is $\sigma_{\rm th}\approx 0.279$ K Å^{-2} which compares favorably with the most recent experimental value[46,47] of $\sigma_{\rm ex}\approx 0.279$ K Å^{-2}.

(2) *Bulk rotons*: Films with a thickness of two or more liquid layers show already a quite clear phonon/roton spectrum. The spectrum starts at finite energy in the long-wavelength limit and contributes, in this momentum regime, very little to the strength. It takes over most of the strength in the regime of the roton minimum.

(3) *Layer rotons*: Films with a strongly layered structure also show excitations (identified as soundlike through their longitudinal current pattern) that propagate essentially within one atomic layer. These excitations have a two-dimensional roton with an energy *below* the bulk roton, and have been identified with a ''shoulder'' in the neutron-scattering spectrum below the ordinary roton minimum.

(4) *Interfacial ripplons*: On very weak substrates, like cesium, one can also have an ''interface ripplon.''[40,42] Its appearance can be understood easily from the following consideration: Consider first a film with *two* free surfaces. Obviously, this film would exhibit two ripplon modes, one at each surface.[48] Now, a weak substrate is moved against one of the two surfaces. The character of the ''ripplon'' at this surface will not change abruptly; rather the circular motion of the particles will be somewhat inhibited, and the energy of the mode will rise. This is precisely what is seen in the energetics and the current pattern of this second mode on Cs. Stronger substrate potentials suppress this interface mode; to distinguish between an ''interfacial ripplon'' and a ''layer phonon'' one must look at the current pattern of the excitation.[42]

The above list of excitations is restricted to modes that can be characterized legitimately by a wave vector $\mathbf{k}_\parallel$ parallel to the surface. To calculate the response to particles impinging normally on the surface, one must also look at the types of excitations *perpendicular* to the surface. These cannot be rigorously classified by a wave number, but one should basically expect standing waves or resonances at discrete frequencies, approaching the excitations of a bulk system as the film becomes thicker. No ripplonic excitations or layer modes should be visible in this case.

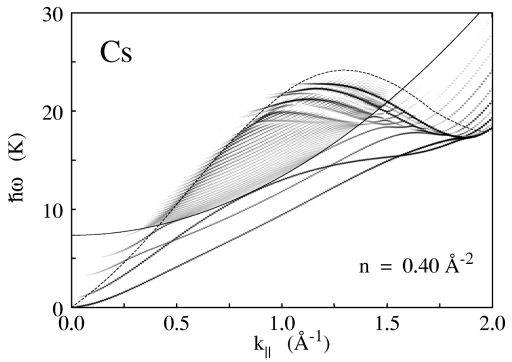

FIG. 4. Dynamic structure function $S(k,\omega)$ in Feynman approximation for a film with coverage of $n=0.400$ Å^{-2} on a Cs substrate and *parallel* momentum transfer. The solid curve shows the continuum boundary $-\mu+\hbar^2 q_\parallel^2/2m_4$ and the dashed line the bulk Feynman spectrum.

The character of excitations is intelligently discussed by examining the *dynamic structure function* $S(\mathbf{k},\omega)$. A general procedure has been developed in Refs. 18,19 to use time-dependent correlations for a quantitative calculation of the dynamic structure function. The simplest version of the theory is analogous to the Feynman approximation;[49,34] the dynamic structure function in that approximation can be calculated directly from the solutions of Eq. (2.7)

$$S(\mathbf{k};\omega)=\left|\int d^3r e^{i\mathbf{r}\cdot\mathbf{k}}\sqrt{\rho_1(\mathbf{r})}\phi_\omega(\mathbf{r})\right|^2, \qquad (3.5)$$

where the $\phi_\omega(\mathbf{r})$ are adjoint states (2.8) of the solutions of Eq. (2.7) for energy $\hbar\omega$. The Feynman approximation has its well-known deficiencies, and methods for its improvement have been derived which provide quantitative agreement with experiments.

Previous work has concentrated on the theoretical interpretation of neutron-scattering experiments, and it was therefore concerned with momenta parallel to the liquid surface. In the present situation we must allow for both parallel and perpendicular momentum transfer. We show in Figs. 4 and 5 the dynamic structure function for parallel and perpendicular momentum transfer. Figure 4 shows the picture familiar from previous work:[18,19,42] a low-lying excitation which can be identified with a ripplon by its dispersion relation and its particle motion, and a high density of states in the roton regime; note that the second lowest dispersion branch corresponds to the interfacial ripplon mentioned above. Note also that the modes below the continuum energy $-\mu_4+\hbar^2 q_\parallel^2/2m_4$ are discrete; they have been broadened by a Lorentzian of the same strength to make them visible.

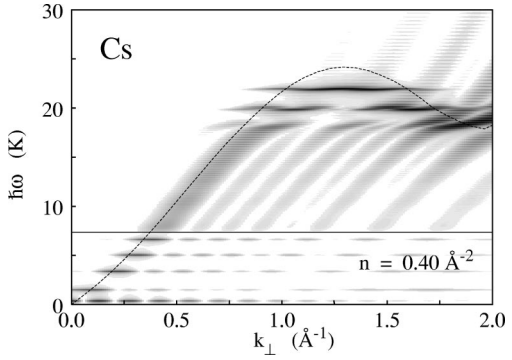

FIG. 5. Same as Fig. 4 for momentum transfer *perpendicular* to the film. The horizontal solid line shows the continuum boundary $-\mu$ and the dashed line the bulk Feynman spectrum.

The situation is quite different for perpendicular scattering. Again, the discrete excitations below the evaporation energy have been broadened. We see a dominant ridge basically along the dispersion relation of a Feynman phonon, and a high density of states in the regime of the roton. The ridge shows a number of ''echoes'' at shorter wavelengths; this is due to the finite-size of the film. But there are — expectedly — no excitations corresponding to the (interfacial) ripplons.

C. Impurity excitations

Calculations of low-lying, bound states including the dynamic self-energy have been discussed extensively in Ref. 20, we list here the most important ones demonstrating both the theoretical consistency as well as the quantitative reliability and highlight their relevance for scattering processes:

(i) When applied to the bulk liquid, the ground state theory produces the correct chemical potentials of ^{3}He and hydrogenic impurities.[50]

(ii) In an inhomogeneous geometry, the *static* theory reproduces the binding energy of the Andreev state.[51] The theory also predicts, even in its most primitive version,[32] the existence of a surface resonance.

(iii) The *dynamic* theory predicts a hydrodynamic effective mass of the Andreev state of $m_H^*/m_I\approx 1.35$, to be compared to the value on 1.38 given by Higley *et al.*[52] somewhat larger than the value of $m_H^*/m_I\approx 1.26$, reported by Valles *et al.*[53] at the lower end of the value $m_H^*/m_I=1.45\pm 0.1$ given by Edwards and Saam.[54] In other words, our theoretical prediction is within the spread of experimental values.

(iv) The energy of the first excited surface state is lowered from about -2.2 to -2.8 K, improving the agreement with the experimental value[51] of approximately -3.2 K notably.

Similar to the obvious existence of interfacial ripplons, one also expects, on weak substrates, the appearance of an interfacial Andreev state. The binding energy of this state was found in Ref. 20 to be approximately -4.3 K, which is somewhat higher than the experimental value[41] of -4.8 K. We attribute the difference to uncertainties in the substrate potential and the certainly oversimplified assumption of a perfectly flat surface. This state—being confined to a smaller area than the surface state—has *always* an energy that is higher than the Andreev state. Although it can, in principle, decay into a surface-bound state, it has negligible overlap and hence its lifetime is practically infinite. With increasing potential strength, the energy of the substrate bound state increases; the state disappears completely on substrates somewhat more attractive than Na. Then, the ''interfacial Andreev state'' turns into a resonance to which a scattering particle can couple. Similar ''resonances'' can be found on Mg substrates even in the *second* layer; we shall return to this point further below.

The two surface-bound states (and, if applicable, the interfacial Andreev state) can be described in the energy regime we are interested in reasonably well by a $t_i(k)=t_i(0)+\hbar^2k^2/2m_3^*$. Above the solvation energy of a ^{3}He

atom, a sequence of impurity states can exist that are spread out throughout the film; the detailed energetics of these states depends on the thickness of the film and the corrugation of the background liquid.

IV. SCATTERING STATES

The background and impurity excitations discussed in the previous section specify the possible energy-loss channels for a scattering particle; we can now turn to the analysis of our results.

The previous work has concentrated on the properties of *bound* impurity atoms, their effective masses, and the lifetime of resonances. Scattering processes are treated within the same theory, imposing asymptotic plane-wave boundary conditions on the solution of the effective Schrödinger equation (2.18):

$$\psi_I(z,\mathbf{r}_\parallel)\rightarrow e^{i\mathbf{k}_\parallel\cdot\mathbf{r}}[e^{-ik_\perp z}+Re^{ik_\perp z}] \quad \text{as} \quad z\rightarrow\infty. \quad (4.1)$$

One of the key quantities of the theory is the elastic reflection coefficient R because it is directly influenced by the coupling of the motion of the impinging particle to the excitations of the quantum liquid. The absolute value of the reflection coefficient can differ from unity only if the self-energy $\Sigma(\mathbf{r},\mathbf{r}',\omega)$ is non-Hermitian. This happens when the energy denominator in the self-energy (2.19) has zeroes; note that the quantum numbers m and r include both the motion of the particles parallel to the surface as well as the discrete or continuous degrees of freedom in the z direction.

Superficially, we appear to be describing a single-particle quantum-mechanical scattering problem. In fact, a number of notions can be carried over from single-particle models and simple phenomenological descriptions can be constructed at the level of a one-body theory. But the actual situation is far richer: Since the scattering film is composed of helium atoms, this is a generically *nonlocal* problem when viewed at the one-body level. Moreover, the film is *dynamic:* the incoming particle may produce excited states of the background. This may result in the capture of the particle and/or the emission of particles in states other than the elastic channel.

A. Quantum reflection

Generally, the amplitude of the wave function of an impinging particle of low energy is suppressed inside an attractive potential by the mismatch of the wavelengths inside and outside the potential if its range is small compared to the wavelength of the particle. As a consequence, the particles are almost totally reflected even if there is dissipation inside the potential [caused by the imaginary part of the self-energy operator (2.19) in our case]

$$1-|R|^2 \propto k_\perp \quad \text{as} \quad k_\perp \rightarrow 0 \quad (4.2)$$

and, consequently, $s\rightarrow 0$ and $r_{\text{inel}}\rightarrow 0$. The effect is called *universal quantum reflection*.[55,56]

Quantum reflection can be described *phenomenologically* in an effective single-particle picture with a complex optical potential. The *many-body* aspect of the problem is to determine the physical origin, the magnitude, and the shape as well as possible nonlocality of that ''optical potential.'' The energy range where quantum reflection is visible in a many-body system like one of those considered here depends sensitively on the energy-loss mechanisms and calls for a quantitative calculation. Even in the limit of zero incident energy, the self-energy (2.19) is non-Hermitian, and thus allows in principle for sticking. Furthermore, this energy range is strongly affected by the long-range features of the substrate potentials.[29,30,15,14]

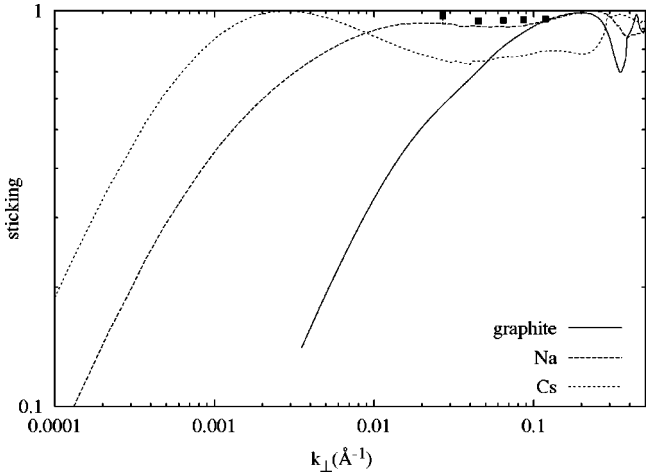

FIG. 6. Sticking on a graphite, Na, and Cs-adsorbed film of $n=0.30$ Å^{-2}. The square boxes in the upper left of the plot are the data of Ref. 7. Note that these data were taken at an impact angle of 60°.

Specifically, in the 3-9 substrate potential models (3.2), the sticking coefficient s depends on the strength C_3 of the potential: For a local potential with the asymptotic form C_3z^{-3} as $z\rightarrow\infty$, one can show[30] that the amplitude of the wave function inside the potential depends linearly on the normal momentum of the incoming particle. Increasing C_3 makes the potential appear smoother for particles with long wavelength, thus increasing the penetration depth and the probability to reach the film. Indeed, a calculation[14–16,28] of the sticking coefficient from the non-Hermitian effective Schrödinger equation (2.18) gives, already in the distorted-wave Born approximation (DWBA), $s\propto k$.

Inelastic scattering is, at low incident energies, only possible by coupling to ripplons. An analysis of the imaginary part of $\Sigma(\mathbf{r},\mathbf{r}',\omega)$ reveals that the contribution of the inelastic channels is proportional to $E^{7/2}$ which gives[29,30] in the DWBA $r_{\text{inel}}\propto E^4$. In other words, inelastic processes are negligible in the low-energy regime.

Although it is not the main thrust of our paper, we have examined the low-energy reflection probabilities. Figure 6 shows three examples for the dependence of the sticking probability $s\approx 1-|R|^2$ on the incident energy for normal incidence. While on graphite adsorbed films, quantum sticking is readily observable in the sense that the sticking coefficient starts to drop monotonically for wavelengths longer than 0.1 Å^{-1}, corresponding to energies less than 0.1 K, the linear dependence of s on k begins only at energies that are two to three orders of magnitude less for Cs adsorbed films (and similarly Mg and Na).

Once the origin and properties of the optical potential for low-energy scattering are understood from a microscopic point of view, one may *a posteriori* construct simple, ana-

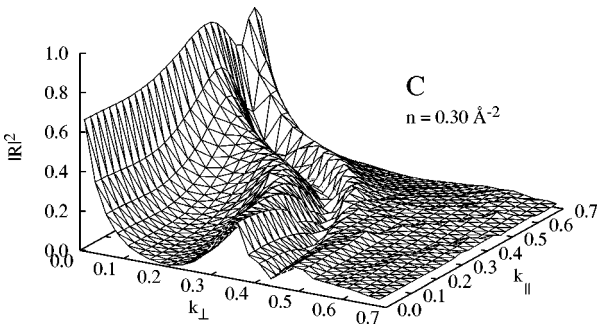

FIG. 7. Dependence of reflection coefficient on wave vector magnitude and angle from a graphite film of density $n = 0.30$ Å^{-2}.

lytic models that provide, within the range suggested by the estimated accuracy of the microscopic picture, some flexibility to examine the dependence of s on features of the optical potential. A simple model consists of a local potential that approaches the substrate potential in the asymptotic region $z \to \infty$ and that is approximated by a square well with a depth estimated from the binding energy of the Andreev state and a width of 15 Å. The energy dissipation term can be included through a localized imaginary part of the typical magnitude of our self-energy. Such a model reproduces qualitatively the large values of s in the mK energy regime. Of course, the model fails to explain the dependence on $\mathbf{k}_\parallel$, see Fig. 11. For completeness, we should also add that retardation should be taken into account for quantitative results below 1–10 mK.[15]

B. Ripplon coupling

''Quantum reflection'' as a generic phenomenon needs only *some* damping mechanism; we now turn to the task of many-body theory to identify and examine the physics that leads to damping. The basic physics is contained in the self-energy (2.19) used in our calculation; it includes the energy loss of an incoming particle with energy $\hbar\omega$ to a background excitation $\hbar\omega_m$, leaving the particle in the state t_r. Within this model, damping is expected to be somewhat underestimated because the possibility to emit two or more phonons has been neglected.

Unless there is negligible overlap of the wave functions, the most efficient energy-loss mechanism is the coupling to the lowest-lying excitation. These lowest-lying excitations of the helium film are the surface waves (*ripplons*), hence one expects that the energy loss of the ^{3}He particle is dominated by the emission of a ripplon. This serves as a *qualitative* argument. However, the reality is more complicated for ^{3}He

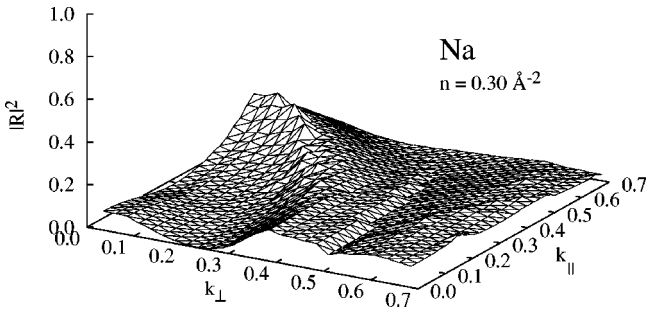

FIG. 9. Same as 7 for a Na film of density $n = 0.30$ Å^{-2}.

scattering because several states are accessible. The condition that an excitation contributes to the imaginary part of the self-energy is that the energy denominator of the self-energy (2.19) vanishes, i.e., $\hbar\omega_m + t_r = \hbar\omega$, and there are several open channels even for vanishing incident energy. First, the particle can, although less efficiently, also couple to higher film excitations and can be promoted into either the second Andreev state or into a bound state in the bulk liquid. The reflection coefficients also depends visibly on the real part of the self-energy, and no quantitative statement can be made without proper treatment of both. The argument holds even at normal incidence, and infinitesimal asymptotic energy of the impinging particle.

We show in Figs. 7–10 a few typical examples of the reflection probability $|R(\mathbf{k}_\parallel, k_\perp)|^2$ for scattering from ^{4}He films adsorbed on graphite, Na, and Cs substrates. In contrast to experiments on atomic scattering of ^{4}He from free ^{4}He surfaces,[7] there is evidently a strong dependence on the parallel wave vector $\mathbf{k}_\parallel$ which needs to be explained in terms of the possible decay channels discussed above. Since it is unlikely that a specific feature is due to a delicate cooperation between film and impurity degrees of freedom, it is legitimate to discuss film- and single-particle excitations independently.

The fact that ripplon coupling is the *dominant* energy-loss mechanism can be verified in various ways. The simplest one is the inspection of the self-energy (2.19): The imaginary part of the self-energy is, with a few exceptions to be discussed below, localized in the surface region where the ripplon lives. The consequence is that at energies below the roton, the wave functions of the impinging particle decays basically within the surface region. The effect can be seen in the wave functions and even better in the probability currents which basically decay within the surface region. A ''resonance'' in Figs. 12 and 13 will be discussed momentarily.

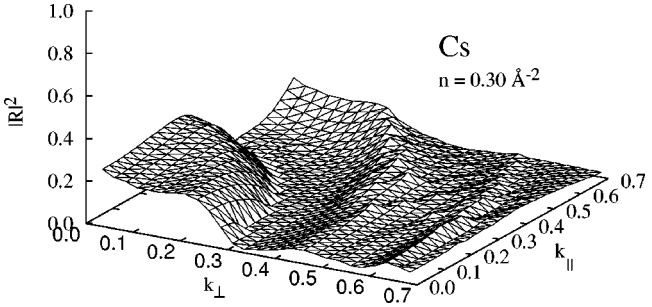

FIG. 8. Same as 7 for a Cs film of density $n = 0.30$ Å^{-2}.

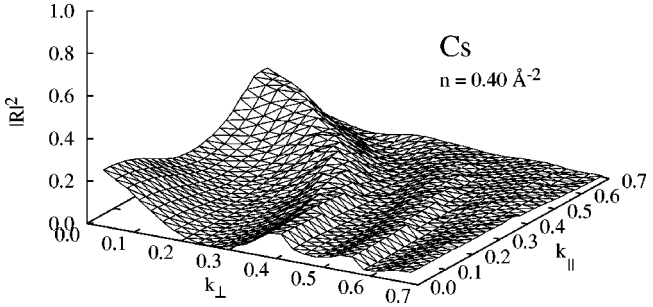

FIG. 10. Same as 7 for a Cs film of density $n = 0.40$ Å^{-2}.

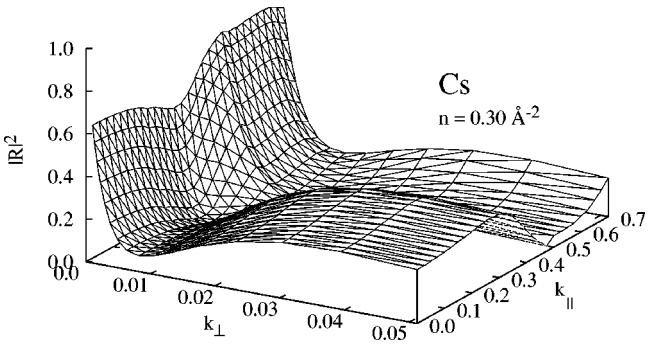

FIG. 11. Fig. 8 is magnified into the regime of low $k_\perp$ to demonstrate that $|R|$ finally approaches unity.

From looking at Figs. 7–10, it appears that quantum reflection is seen only for the graphite substrate. As explained above, this is simply a consequence of the fact that the reflection becomes visible only at much lower energies on the alkali-metal substrates. To demonstrate this, we have magnified in Fig. 11 the low-energy region for the Cs substrate; consistent with Fig. 6, it is seen that the reflectivity starts to rise at impact energies of less than 0.001 K.

C. Single-particle resonances

While the generic many-body aspect of all scattering and in particular damping mechanisms must be kept in mind, one-body pictures can occasionally—as above for quantum reflection—provide useful paradigms in cases where the process under consideration can be described in terms of the degrees of freedom of a single particle. Such an effect is the coupling to *single-particle resonances*. A convenient and physically illustrative definition of a resonance at an energy $\hbar\omega$ is a large probability $|\psi_I(\mathbf{r},\omega)|^2$ in the region of interaction. The resulting large dissipation will render $|R(\omega)|^2$ small.

The peak of the wave function close to the substrate at $k_\perp \approx 0.4$ Å^{-1} and $z \approx 1.2$ Å shown in Fig. 12 is a very pronounced example of such a resonance. It displays exactly the phenomenon discussed above that the interfacial Andreev state turns into a resonance as the substrate strength is increased. The energy of this resonance is significantly reduced by the coupling to *virtual* phonons: The resonance has an energy of approximately 6 K in the static approximation (2.12). Including the dynamic self-energy corrections through the (real part of) $\Sigma(\omega)$, the resonance energy drops to approximately 1.3 K. The energy where the wave function has a strong peak in the vicinity of the substrate coincides with that of the dip in the reflection coefficient. Figure 12 shows this for the special case of zero parallel momentum, but the agreement between the peak of the wave function and the minimum of the reflection probability persists at all parallel momenta. Also seen clearly in Fig. 12 is the change in the phase of the wave as the resonance is crossed as a function of energy.

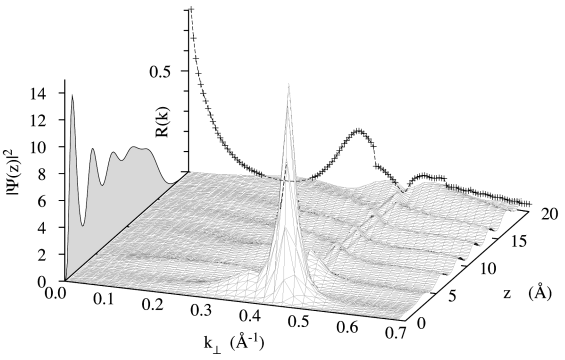

FIG. 12. The figure shows the wave function $|\psi(z)|^2$ of a ^{3}He as a function of distance z and perpendicular wave number $p_\perp$ for normal incidence. The left face shows, for reference, the density profile of the film and the back face the reflection coefficient $R(k_\perp)$. The substrate is graphite *plus* two solid helium layers, the surface coverage is $n = 0.300$ Å^{-2}.

The elliptic ridge of the reflection coefficient as a function of $(k_\perp, k_\parallel)$ can be explained by the coupling of the interfacial Andreev resonance discussed above to the virtual excitations of the film. This has the consequence that the resonance acquires an effective mass[20] $m^*_{\rm res}$. At zero parallel momentum, the position of the dip in the reflection coefficient agrees with the location of the resonance seen in Fig. 12. The shape of the ridge can be explained by assuming that *all* of the energy of the impinging particle is deposited in that resonance. Energy conservation and momentum conservation *parallel* to the substrate then leads to the relationship

$$\epsilon_{\rm res} = \frac{\hbar^2 k_\perp^2}{2m_3} + \frac{\hbar^2 k_\parallel^2}{2m_3}\left[1 - \frac{m_3}{m^*_{\rm res}}\right], \tag{4.3}$$

where $\epsilon_{\rm res}$ is the energy of the resonance. Following the peak of the wave function in the resonance in the $(k_\perp, k_\parallel)$ plane leads, within the accuracy that can be expected from such a relatively crude argument, to the same conclusion. Basically—and expectedly—the same resonances occur at other surface coverages; the precise location of the dip in the reflection varies due to the multitude of other open scattering channels. A similar resonance occurs in the more strongly attractive Mg substrates, the corresponding wave functions are shown in Fig. 13. In this case, one finds a second resonance in the second layer which is, however, less pronounced. A list of energies and effective masses is given, together with the values for the Andreev state and the results of Ref. 20 of the bound states, in Table I. The effective masses were obtained by fitting the curve defined by Eq. (4.3) to reproduce the location of the peak of the wave function within the visible region. As pointed out above, the weaker substrate Cs has a bound state to which the scattering particle cannot couple, whereas the Na substrate is a marginal case.

In all cases considered here we have found a significant dependence of the reflection coefficient $|R|$ on the *parallel* momentum, cf. Figs. 7–10. Such a feature cannot be explained within a local, complex single-particle model, is also not seen in experiments on ^{4}He scattering off ^{4}He films/surfaces.[7] The feature is most pronounced on graphite and Mg substrates, cf. Fig. 7.

Also for the other substrates (see Figs. 8, 9, and 10), $R(\omega)$ depends on the parallel component of the momentum. One sees similar, but broader ridges in the reflection coefficient, but *no* sharp peaks in the wave function, cf. Fig. 14. The effect can also be explained by the features of the impurity

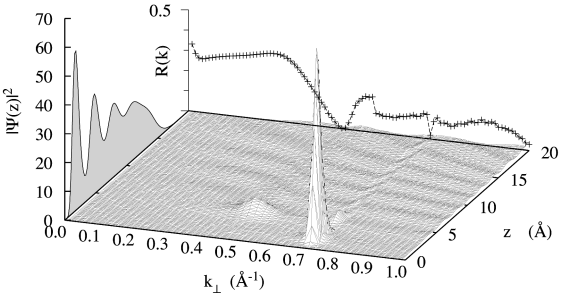

FIG. 13. Same as 12 for a film of $n=0.300$ Å^{-2} on a Mg substrate.

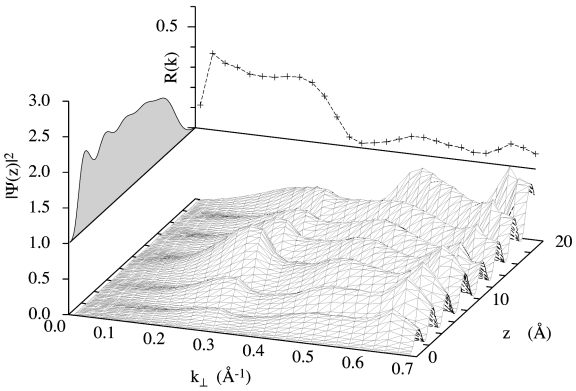

FIG. 14. Same as 12 for a film of $n=0.300$ Å^{-2} on a Cs substrate.

states within the film. But this time, the impurity states are *not* localized but are extended states that will, with increasing film thickness, develop to ^{3}He states dissolved in the ^{4}He liquid. Consistent with this picture, the energy of the resonances in Na and Cs adsorbed films decreases with increasing surface coverage n, until they become bound states, cf. Fig. 16. This slipping below the threshold $E=0$ is best seen in the phase shift at $E\to 0$, which jumps whenever this occurs (in case of Cs: at $n=0.330$ and 0.380 Å^{-2}).

D. Roton coupling

The presence of roton excitations affects the scattering properties at two levels. First, at *all* energies, the coupling to virtual rotons is a significant contribution to the *real part* of the self-energy; omitting these contributions by, for example, restricting the state sums in the self-energy (2.19) to energies below the roton minimum, leads to reflection coefficients that are, even at energies well below the roton minimum, about a factor of 2 smaller than when excitations in the roton regime are included; cf. Fig. 15. This is to some extent plausible since the roton is a reflection of the short-range structure of the system which is dominated by the core repulsion, and such effects should make the film look ''stiffer.''

At higher energies, the coupling to roton excitations also opens a new damping mechanism. As seen in Fig. 5, ''roton-like'' excitations appear also for film excitations perpendicular to the surface, and the impinging particle can couple to these excitations. In our calculations, the effect of roton coupling should become visible at an energy of about 15 K, this is because we have used a Feynman spectrum in the energy denominator of Eq. (2.19). In previous work,[19] we have scaled the energy denominators in the self-energy by an amount such that the roton is placed at roughly the right energy. We have refrained from this phenomenological modification since this procedure would also scale the ripplon away from its correct value which is already obtained in the Feynman approximation.

Above 15 K, the film loses its elastic reflectivity for ^{3}He atoms completely. There is, of course, still the possibility of some inelastic scattering, but we consider this scenario unlikely from our experience with the propagation of ^{3}He impurities in *bulk* ^{4}He.[50] Hence, we expect that ^{3}He atoms will be completely absorbed by ^{4}He films when the impact energy is above the energy of the bulk roton. The effect is also seen quite clearly in the wave function of the scattering particle which does not penetrate into the film at all at energies above that of the roton.

TABLE I. Resonance energies and effective masses of the interfacial Andreev state on various substrates. The first line gives, for reference, the data of the Andreev state at the free surface, and the second the interfacial Andreev state on a Cs substrate (From Ref. 20). The last three lines give the results obtained here from scattering properties. Energies are given in K, the row labeled with ''C'' refers to the graphite *plus* two solid layers of ^{4}He model used in this work.

Substrate	Energy	m^*/m_3
	-5.4	1.3
Cs	-4.3	1.7
C	1.3 ± 0.3	1.7 ± 0.3
Mg	4.3 ± 0.5	1.6 ± 0.2

V. SUMMARY

We have set in this paper the basic scenario for calculations of atom scattering processes from inhomogeneous ^{4}He.

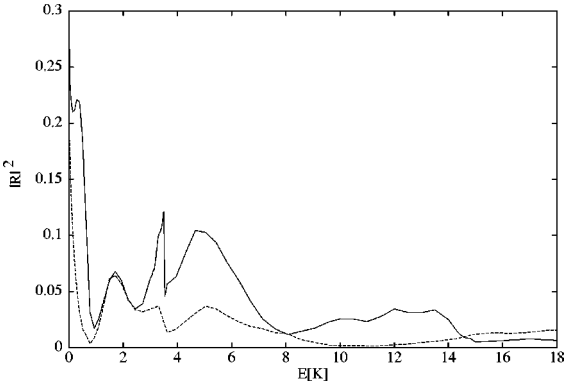

FIG. 15. Reflection coefficient $|R|^2$ for normal incidence on a film with $n=0.300$ Å^{-2} on a Cs-adsorbed film. The solid line is the result when all relevant intermediate states are kept in the state sums (2.19), whereas the dashed line is the result when the sum over intermediate states is truncated below the roton minimum. A new scattering channel opens at 3.5 K.

This work parallels similar research on scattering of ^{4}He atoms[24] and also provides the groundwork for applications on the presently active area of atom scattering from ^{4}He clusters.

Technically, the calculations presented here are somewhat simpler than those for ^{4}He atom scattering[24] (since the Hartree impurity spectra appearing in the energy denominators in Eq. (2.19) are decoupled in parallel and perpendicular motion in contrast to the ripplon/phonon/roton spectra) which enabled us to do a systematic study of the dependence of the reflection coefficient on the parallel momentum.

When applicable, our general conclusions are very similar to those that we have drawn for ^{4}He atom scattering: Most of the physics happens due to ripplon coupling, the wave function is substantially damped in the surface region. ''Quantum reflection'' does not come to bear until energies as low as 0.1 K on a graphite substrate, and 0.01 K or less on alkali metals. A second damping mechanism happening at higher energies is the coupling to rotons, this effect dampens the impurity motion completely; an equivalent effect is expected, and found, in bulk ^{4}He.

An aspect specific to ^{3}He scattering is the coupling to single-particle resonances within the film; such an effect will not be seen for ^{4}He scattering. We have demonstrated that the properties of the remaining reflected particles are directly influenced by the features of the impurity states within these films and that scattering experiments can directly measure the energy and the ''effective mass'' of these resonances. Fully acknowledging the experimental difficulty of the task, we hope that these findings will inspire further measurements on ^{3}He scattering off ^{4}He surfaces and films.

Unfortunately it is difficult to make direct comparisons with experiments available today.[7] One reason is that we are with our calculations apparently still too far from the bulk limit that a comparison is meaningful. This is most clearly seen in the oscillatory dependence of the reflection coefficient on the energy of the incoming particle even in a case if a relatively thick film without localized resonances within the film (Fig. 14). There is also still pronounced nonmonotonic dependence of the reflection coefficient on the surface coverage, cf. Fig. 16.

Further applications of our work are twofold: One is the application to scattering of hydrogen isotopes off ^{4}He surface. While experimental efforts in this area have been significantly stronger,[11–13] the situation is less rich: The H impurity is only very weakly bound and can lose its energy only to the ripplon, in other words the imaginary part of the self-energy (2.19) comes from one state only. Moreover, the H atom must overcome a potential barrier of about 10 K to penetrate into the bulk liquid which makes the coupling to any interior degrees of freedom negligible.

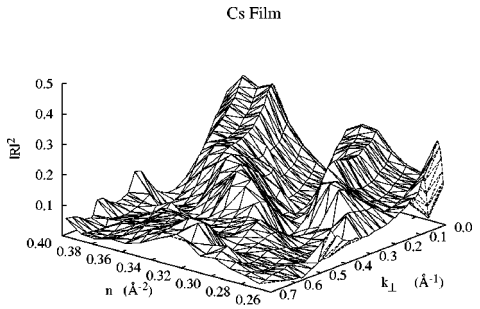

FIG. 16. Reflection coefficient $|R|^2$ for normal incidence on a sequence films with surface coverages between $n=0.26$ and 0.39 Å^{-2} on a Cs-adsorbed film.

Similarly interesting is the possibility of scattering experiments of both ^{3}He and ^{4}He atoms off ^{4}He *droplets.* These experiments, to be carried out in the energy regime of a few tenth to a few degrees, would also couple to both surface and volume modes and should also more clearly display the coupling to excitations inside the droplets. In the spherical geometry, inelastic processes of the kind described here cannot occur at low energy because the continuous quantum number $\mathbf{k}_\parallel$ is replaced by the discrete angular momentum. Hence, all low-lying modes are discrete and the energy denominator of Eq. (2.19) will normally be nonzero, in other words the self-energy is Hermitian. Moreover, these systems are not contaminated by substrate effects and should therefore allow for a cleaner interpretation of the results. We have learned that such scattering experiments have meanwhile been performed[57] and show indeed the expected coupling of ^{3}He particles to rotonlike excitations inside the droplets.

Such experiments and calculations would also provide an ideal scenario to test ideas and procedures established in nuclear physics in a much better controlled and—in terms of the underlying Hamiltonian—better understood physics. Calculations in this direction are in progress and will be published elsewhere.

ACKNOWLEDGMENTS

This work was supported in part by the Austrian Science Fund under Project No. P11098-PHY. We thank S. E. Campbell, R. B. Hallock, J. Klier, and M. Saarela for valuable discussions.

[1] A. F. G. Wyatt, M. A. H. Tucker, and R. F. Cregan, Phys. Rev. Lett. **74**, 5236 (1995).
[2] M. A. H. Tucker and A. F. G. Wyatt, J. Low Temp. Phys. **100**, 105 (1995).
[3] M. A. H. Tucker and A. F. G. Wyatt, Physica B **194-196**, 549 (1994).
[4] R. F. Cregan, M. A. H. Tucker, and A. F. G. Wyatt, J. Low Temp. Phys. **101**, 531 (1995).
[5] D. O. Edwards *et al.*, Phys. Rev. Lett. **34**, 1153 (1975).
[6] D. O. Edwards and P. P. Fatouros, Phys. Rev. B **17**, 2147 (1978).
[7] V. U. Nayak, D. O. Edwards, and N. Masuhara, Phys. Rev. Lett. **50**, 990 (1983).
[8] D. R. Swanson and D. O. Edwards, Phys. Rev. B **37**, 1539 (1988).
[9] D. O. Edwards, P. P. Fatouros, and G. G. Ihas, Phys. Lett. **59A**, 131 (1976).
[10] H. P. Godfried *et al.*, Phys. Rev. Lett. **55**, 1311 (1985), measuring of adsorbtion energies and recombination rate.

[11] J. J. Berkhout, E. J. Wolters, R. van Roijen, and J. T. M. Walraven, Phys. Rev. Lett. **57**, 2387 (1986).
[12] J. M. Doyle *et al.*, Phys. Rev. Lett. **67**, 603 (1991).
[13] I. A. Yu *et al.*, Phys. Rev. Lett. **71**, 1589 (1993).
[14] C. Carraro and M. W. Cole, Phys. Rev. B **45**, 12 930 (1992).
[15] C. Carraro and M. W. Cole, Z. Phys. B **98**, 319 (1995).
[16] E. R. Bittner and J. C. Light, J. Chem. Phys. **102**, 2614 (1995).
[17] B. E. Clements, J. L. Epstein, E. Krotscheck, and M. Saarela, Phys. Rev. B **48**, 7450 (1993).
[18] B. E. Clements *et al.*, Phys. Rev. B **50**, 6958 (1994).
[19] B. E. Clements, E. Krotscheck, and C. J. Tymczak, Phys. Rev. B **53**, 12 253 (1996).
[20] B. E. Clements, E. Krotscheck, and M. Saarela, Phys. Rev. B **55**, 5959 (1997).
[21] E. Krotscheck, M. Saarela, and J. L. Epstein, Phys. Rev. B **38**, 111 (1988).
[22] E. Krotscheck, M. Saarela, and J. L. Epstein, Phys. Rev. Lett. **61**, 1728 (1988).
[23] J. L. Epstein, E. Krotscheck, and M. Saarela, Phys. Rev. Lett. **64**, 427 (1990).
[24] C. E. Campbell, E. Krotscheck, and M. Saarela, Phys. Rev. Lett. **80**, 2169 (1998).
[25] J. W. Halley, C. E. Campbell, C. F. Giese, and K. Goetz, Phys. Rev. Lett. **71**, 2429 (1993).
[26] C. E. Campbell and J. W. Halley, Physica B **194-196**, 533 (1994).
[27] A. K. Setty, J. W. Halley, and C. E. Campbell, Phys. Rev. Lett. **79**, 3930 (1997).
[28] D. P. Clougherty and W. Kohn, Phys. Rev. B **46**, 4921 (1993).
[29] W. Brenig, Z. Phys. B **36**, 227 (1980).
[30] J. Bölheim, W. Brenig, and J. Stuzki, Z. Phys. B **48**, 43 (1982).
[31] G. P. Brivio, T. B. Grimley, and G. Guerra, Surf. Sci. **320**, 344 (1994).
[32] E. Krotscheck, Phys. Rev. B **32**, 5713 (1985).
[33] E. Feenberg, *Theory of Quantum Liquids* (Academic, New York, 1969).
[34] C. C. Chang and M. Cohen, Phys. Rev. A **8**, 1930 (1973).
[35] E. Zaremba and W. Kohn, Phys. Rev. B **15**, 1769 (1977).
[36] M. W. Cole, D. R. Frankl, and D. L. Goodstein, Rev. Mod. Phys. **53**, 199 (1981).
[37] P. J. Nacher and J. Dupont-Roc, Phys. Rev. Lett. **67**, 2966 (1991).
[38] K. S. Ketola, S. Wang, and R. B. Hallock, Phys. Rev. Lett. **68**, 201 (1992).
[39] P. Taborek and J. E. Rutledge, Phys. Rev. Lett. **68**, 2184 (1992).
[40] J. Klier and A. F. G. Wyatt, Czech. J. Phys. Suppl. **46**, 439 (1996).
[41] D. Ross, P. Taborek, and J. E. Rutledge, Phys. Rev. Lett. **74**, 4483 (1995).
[42] B. E. Clements, E. Krotscheck, and C. J. Tymczak, J. Low Temp. Phys. **107**, 387 (1997).
[43] H. J. Lauter, H. Godfrin, V. L. P. Frank, and P. Leiderer, in *Excitations in Two-Dimensional and Three-Dimensional Quantum Fluids*, Vol. 257 of *NATO Advanced Study Institute, Series B: Physics*, edited by A. F. G. Wyatt and H. J. Lauter (Plenum, New York, 1991), pp. 419–427.
[44] H. J. Lauter, H. Godfrin, V. L. P. Frank, and P. Leiderer, Phys. Rev. Lett. **68**, 2484 (1992).
[45] H. J. Lauter, H. Godfrin, and P. Leiderer, J. Low Temp. Phys. **87**, 425 (1992).
[46] G. Deville, P. Roche, N. J. Appleyard, and F. I. B. Williams, Czech. J. Phys. Suppl. **46**, 89 (1996).
[47] P. Roche, G. Deville, N. J. Appleyard, and F. I. B. Williams, J. Low Temp. Phys. **106**, 565 (1997).
[48] E. Krotscheck, Phys. Rev. B **31**, 4258 (1985).
[49] R. P. Feynman, Phys. Rev. **94**, 262 (1954).
[50] M. Saarela and E. Krotscheck, J. Low Temp. Phys. **90**, 415 (1993).
[51] D. T. Sprague, N. Alikacem, P. A. Sheldon, and R. B. Hallock, Phys. Rev. Lett. **72**, 384 (1994).
[52] R. H. Higley, D. T. Sprague, and R. B. Hallock, Phys. Rev. Lett. **63**, 2570 (1989).
[53] J. M. Valles, Jr., R. H. Higley, B. R. Johnson, and R. B. Hallock, Phys. Rev. Lett. **60**, 428 (1988).
[54] D. O. Edwards and W. F. Saam, in *Progress in Low Temperature Physics*, edited by D. F. Brewer (North-Holland, New York, 1978), Vol. 7A, pp. 282–369.
[55] J. E. Lennard-Jones, F. R. Strachan, and A. F. Devonshire, Proc. R. Soc. London **156**, 6 (1936).
[56] J. E. Lennard-Jones, F. R. Strachan, and A. F. Devonshire, Proc. R. Soc. London **156**, 29 (1936).
[57] J. Harms and P. Toennies (private communication).